

The high energy tail of γ -ray burst 941017: Comptonization of synchrotron self absorbed photons

Asaf Pe'er¹ and Eli Waxman¹

ABSTRACT

The recent detection of an unusually hard spectral component in GRB941017 extending to ≥ 200 MeV is hard to explain as a synchrotron emission from shock-accelerated electrons. It was argued to imply acceleration of protons to ultra-high energy. We show here that the "high energy tail" can be explained as emission from shock-accelerated electrons in the early afterglow epoch, taking into account the effect of synchrotron self-absorption. High energy observations set in this case stringent constraints on model parameters: A lower limit to the total explosion energy $E \gtrsim 5 \times 10^{53}$ erg (assuming spherical symmetry); An upper limit to the density of gas surrounding the explosion, $n \lesssim 10^{-1}(E/10^{54}\text{erg})\text{cm}^{-3}$; a lower limit to the expansion Lorentz factor $\Gamma_i \gtrsim 200$; and an upper limit to the fraction of thermal energy carried by the magnetic field behind the shock driven into the surrounding medium, $\epsilon_{B,f} \leq 10^{-4}$. Such constraints can not be inferred from keV–MeV data alone. The unusually low value of $\epsilon_{B,f}$ may account for the rareness of GRB941017-type high energy tails. Tighter constraints on model parameters may be obtained in the future from optical and sub-TeV observations.

Subject headings: gamma rays:bursts — gamma rays: theory — radiation mechanism:nonthermal

1. Introduction

In fireball models of GRBs (Piran 2000; Mészáros 2002; Waxman 2003) the energy released by an explosion is converted to kinetic energy of a thin baryonic shell expanding at an ultra-relativistic speed. The GRB is most likely produced by internal shocks within the expanding shell. At a later stage, the shell impacts on surrounding gas, driving an ultra-relativistic shock into the ambient medium. This shock continuously heats fresh gas and accelerates relativistic electrons, which produce synchrotron emission that account for the long term X-ray, optical and radio emission (the "afterglow") following the GRB. The initial interaction of fireball ejecta with surrounding gas produces a reverse shock which propagates into and decelerates the fireball ejecta (Mészáros, Rees & Papathanassiou 1994). As the reverse shock crosses the ejecta, it erases the

¹Physics faculty, Weizmann Institute of Science, Rehovot 76100, Israel; asaf@wicc.weizmann.ac.il

memory of the initial conditions, and the expansion then approaches the Blandford-McKee self-similar solutions (Blandford & McKee 1976), where the expansion Lorentz factor decreases with radius as $\Gamma_{\text{BM}} = (17E/16\pi nm_p c^2)^{1/2} r^{-3/2}$. Here E is the total explosion energy (assuming spherical symmetry), n is the number density of the ambient medium.

The duration T of the stage of transition to self-similar expansion, during which the reverse shock "lives", is comparable to the longer of the two time scales set by the initial conditions (Waxman 2003): The (observed) GRB duration T_{GRB} and the (observed) time T_{Γ} at which the self-similar Lorentz factor Γ_{BM} equals the original ejecta Lorentz factor Γ_i , $\Gamma_{\text{BM}}(T_{\Gamma}) = \Gamma_i$. Since the characteristic time over which radiation emitted by the fireball at radius r is observed by a distant observer is $\approx r/4\Gamma^2 c$ (Waxman 1997), T is determined by (Waxman 2003)

$$T \approx \max \left[T_{\text{GRB}}, 10 \left(\frac{E_{53}}{n_{-1}} \right)^{1/3} \left(\frac{\Gamma_i}{300} \right)^{-8/3} \text{ s} \right], \quad (1)$$

where $E = 10^{53} E_{53}$ erg and $n = 0.1 n_{-1}$ cm $^{-3}$. Note, that the duration is increased by a factor $1+z$ for a burst at redshift z .

Observations of GRB941017 show two distinct spectral components (González *et al.* 2003): A low energy component, with photon energies $\varepsilon_{\gamma} \lesssim 3$ MeV, and a high energy component, $\varepsilon_{\gamma} \gtrsim 3$ MeV. The low energy component shows rapid variability, has a characteristic GRB spectrum peaking at $\varepsilon_{\gamma} \sim 0.5$ MeV, and decays over ~ 100 s. The high energy component has a very hard spectrum, number of photons per unit photon energy $dn_{\gamma}/d\varepsilon_{\gamma} \propto \varepsilon_{\gamma}^{-1}$, and persists over ~ 200 s. The different temporal behavior suggests that the two components are produced in different regions of the expanding fireball. The characteristics of the low energy component suggest that it is produced by internal shocks, similar to other GRBs. The temporal behavior of the high energy component suggests that it is produced during the transition to self-similar expansion.

The hard, $dn_{\gamma}/d\varepsilon_{\gamma} \propto \varepsilon_{\gamma}^{-1}$, spectrum is difficult to account for in models where emission is dominated by shock accelerated electrons (González *et al.* 2003; Granot & Guetta 2003). This has lead González *et al.* to suggest that the high energy tail is due to electromagnetic cascades initiated by the interaction of photons with ultra-high energy shock-accelerated protons (Waxman 1995; Vietri 1995; Böttcher & Dermer 1998; Totani 1998; Waxman & Bahcall 2000). We present here an alternative explanation: Electrons accelerated in the forward shock inverse-Compton scatter optical photons, emitted by the reverse shock electrons, to create the observed spectra. The key point, which allows to reproduce the observed hard spectrum, is the modification of the synchrotron spectrum by self-absorption in the reverse shock. We show that this effect allows to reproduce the observed hard, high energy tail also in the internal shock phase (see § 4). However, we consider the latter explanation less likely, due to the weak time dependence of the high energy component.

This paper is organized as follows. In § 2 we briefly discuss the dynamics of transition to self-similar expansion and the plasma conditions during the transition. In § 3 we analytically derive the constraints imposed on model parameters by the observation of a high energy tail. In § 4 we present results from detailed numerical calculations of the spectrum, which demonstrate

that the observed spectrum may be reproduced when the constraints derived in § 3 are satisfied. A numerical calculation of the spectrum is essential, since the spectral shape near the inverse-Compton up-scattered self-absorption frequency is not well described by simple power-law approximations. Our analysis improves on that of Granot & Guetta (2003), by taking into account the effects of synchrotron self-absorption and of emission from the forward shock electrons, and by carrying out detailed numerical calculations of the resulting spectra. Our conclusions are summarized in § 5.

2. The transition to self-similar expansion

During the transition, plasma shocked by the reverse shock expands with Lorentz factor close to that given by the self-similar solution,

$$\Gamma \simeq 140 \left(\frac{E_{53}}{n_{-1}} \right)^{1/8} T_2^{-3/8}, \quad (2)$$

where $T = 10^2 T_2$ s. The unshocked fireball ejecta propagate with the original expansion Lorentz factor, $\Gamma_i > \Gamma$. The forward shock which propagates into the ambient medium is highly relativistic, propagating with Lorentz factor $\approx \Gamma_{\text{BM}}$, while the reverse shock is mildly relativistic, propagating into the ejecta with Lorentz factor $\approx 1 + \Gamma_i/\Gamma_{\text{BM}}$.

The radiation luminosity and spectrum are determined, for given E , n and Γ_i , by the fraction ϵ_B (ϵ_e) of shock thermal energy carried by magnetic field (relativistic electrons), and by the shape of the electron distribution function, which is commonly assumed to be a power law of index $p \equiv -d \ln n_e / d \ln \gamma_e$ for electron Lorentz factors γ_e exceeding γ_{em} . The values of the parameters ϵ_B and ϵ_e can not be determined from first principles, since the micro-physics of collisionless shocks which determines them is not fully understood. We therefore leave them as free parameters in the following analysis, and derive the constraints imposed on them by observations. Since the forward shock is highly relativistic, while the reverse shock is only mildly relativistic, we allow different values for ϵ_B and ϵ_e in the two shocks. Thus, for example, $\gamma_{em,r} = \epsilon_{e,r} (m_p/m_e) (\Gamma_i/\Gamma_{\text{BM}}) (p-2)/(p-1)$ for the reverse shock, and $\gamma_{em,f} = \epsilon_{e,f} (m_p/m_e) \Gamma_{\text{BM}} (p-2)/(p-1)$ for the forward shock (for $p > 2$).

Synchrotron emission from electrons accelerated in the reverse shock typically peaks in the optical/IR band (Mészáros & Rees 1997; Sari & Piran 1999),

$$\varepsilon_{\gamma, \text{RS}}^{\text{ob.}} \approx \hbar \Gamma \gamma_{em,r}^2 \frac{3}{2} \frac{qB}{m_e c} = 0.2 n_{-1}^{1/2} \Gamma_{i,2.5}^2 \epsilon_{e,r,-1}^2 \epsilon_{B,r,-2}^{1/2} \text{ eV.} \quad (3)$$

Here, $\Gamma_i = 10^{2.5} \Gamma_{i,2.5}$, $\epsilon_{e,r} = 10^{-1} \epsilon_{e,r,-1}$, and $\epsilon_{B,r} = 10^{-2} \epsilon_{B,r,-2}$. This energy is similar to the photon energy ε_{ssa} at which the optical depth for synchrotron self-absorption in the reverse shock equals unity,

$$\varepsilon_{\text{ssa}}^{\text{ob.}} \approx 0.8 E_{53}^{1/3} n_{-1}^{1/3} T_2^{2/3} \Gamma_{i,2.5}^{1/3} \epsilon_{e,r,-1}^{2/3} \epsilon_{B,r,-2}^{1/3} \text{ eV.} \quad (4)$$

Denoting by $\gamma_{c,r}$ the Lorentz factor of reverse shock electrons for which the synchrotron cooling time is comparable to the ejecta expansion time, and assuming that electrons with $\gamma > \gamma_{c,r}$ emit

nearly 100% of their energy during the dynamical time, the photon energy density is (for $p = 3$)

$$u_{ph,syn,r} \approx 2 \frac{\gamma_{em,r}}{\gamma_{c,r}} \epsilon_{e,r} u = 2.5 \times 10^{-2} E_{53}^{1/2} n_{-1}^{3/2} T_2^{-1/2} \Gamma_{i,2.5} \epsilon_{e,r,-1}^2 \epsilon_{B,r,-2} \text{ erg cm}^{-3}, \quad (5)$$

where the thermal energy density is $u = 4\Gamma_{\text{BM}}^2 n m_p c^2$.

3. Constraints on model parameters

Electrons accelerated in the forward shock, with Lorentz factors $\gamma_{em,f} \sim \epsilon_{e,f} (m_p/m_e) \Gamma_{\text{BM}}/2 \sim 10^{4.5}$, inverse-Compton scatter the optical photons, boosting their energy by $\sim \gamma_{em,f}^2$ to $\sim 1 \text{ GeV}$. The spectral shape of inverse-Compton scattered photons at observed energy range, $\varepsilon_\gamma < 1 \text{ GeV}$, is similar to the spectral shape of the reverse shock synchrotron spectrum at $\varepsilon_\gamma \lesssim 1 \text{ eV}$, as the energy of all photons is boosted by roughly the same factor $\sim \gamma_{em,f}^2$. However, the spectral shape is expected to smoothen somewhat, because Compton scattering is not exactly monochromatic. The low energy synchrotron spectrum is affected by self-absorption (Eq. 4). The optical depth increases as photon energy decreases, leading to a thermal spectrum $dn_\gamma/d\varepsilon_\gamma \propto \varepsilon_\gamma^1$ at $\varepsilon_\gamma \ll \varepsilon_{\text{ssa}}$. This spectrum is harder than observed. However, it becomes softer as ε_γ approaches $\varepsilon_{\text{ssa}} \approx \varepsilon_{\gamma,\text{RS}}$, which may allow to produce a spectrum consistent with observations.

Thus, in order to explain the observed spectrum as due to inverse-Compton scattering of self-absorbed synchrotron photons, the following conditions must be met:

1. The energy of synchrotron photons for which the reverse shock optical depth is unity, $\varepsilon_\gamma = \varepsilon_{\text{ssa}}$, should be increased via inverse-Compton scattering by the lowest energy electrons in the forward shock, $\gamma_e = \gamma_{em,f}$, to $\approx 200 \text{ MeV}$, i.e.

$$\gamma_{em,f}^2 \varepsilon_{\text{ssa}} \gtrsim 200 \text{ MeV}. \quad (6)$$

2. The lowest energy electrons in the forward shock, $\gamma_e = \gamma_{em,f}$, should lose energy (via synchrotron and inverse-Compton scattering) on a time scale longer than T . If this condition is not met, cooling of the electrons would lead to a spectrum $d \ln n_e / d \ln \gamma_e \approx -2$ at $\gamma_e < \gamma_{em,f}$, which will produce an inverse-Compton spectrum $dn_\gamma/d\varepsilon_\gamma \propto \varepsilon_\gamma^{-3/2}$ below 1 GeV, softer than observed. This condition can be written in the form

$$\begin{aligned} \gamma_{c,f} &\geq \gamma_{em,f}, \\ \gamma_{IC,c,f} &\geq \gamma_{em,f}, \end{aligned} \quad (7)$$

where $\gamma_{IC,c,f}$ ($\gamma_{c,f}$) is the Lorentz factor of forward shocked electrons for which the cooling time due to inverse-Compton (synchrotron) emission is comparable to the expansion time. The inverse-Compton cooling time is estimated via $t_{\text{cool},IC} = t_{\text{cool},syn} (u_{B,f}/u_{ph,syn,r})$, where $u_{B,f} = \epsilon_{B,f} u$ is the energy density in the magnetic field at the forward shock.

3. Synchrotron emission from the forward shock electrons, as well as inverse-Compton emission from reverse shock electrons, should not exceed the observed flux at the 10 KeV to 1 MeV range. These requirements can be met by requiring either (a) The flux to be lower than observed, or (b) The photons to be emitted below 10 KeV. For synchrotron emission from the forward shock this implies either (a)

$$\frac{L_{IC,f}}{L_{syn,f}} = \frac{u_{ph,syn,r}}{u_{B,f}} > 10^3 \quad (8)$$

or (b)

$$\varepsilon_{\gamma,FS}^{ob.} \lesssim 1 \text{ KeV}. \quad (9)$$

For inverse-Compton emission from the reverse shock it implies either (a)

$$\frac{L_{IC,f}}{L_{IC,r}} = \frac{\epsilon_{B,r}}{\epsilon_{e,r}} \frac{\gamma_{c,r}}{\gamma_{em,r}} \gamma_{em,f}^2 \tau_{T,f} > 10^3 \quad (10)$$

or (b)

$$\varepsilon_{\gamma,IC,RS}^{ob.} = \varepsilon_{\gamma,RS}^{ob.} \gamma_{em,r}^2 \lesssim 1 \text{ KeV}. \quad (11)$$

A lengthy, but straight forward, manipulation of the above constraints lead to the following constraints on model parameters²:

$$\begin{aligned}
 a. \quad E_{53} &\geq 4 & T_2^{3/2}, \\
 b. \quad \left(\frac{E_{53}}{n-1}\right) &\geq 50 & T_2^4, \\
 c. \quad \epsilon_{e,r,-1} &\geq 1.5 E_{53}^{-1} & T_2^{5/2}, \\
 d. \quad \epsilon_{B,r,-2} &\lesssim 15 & T_2^{37/8}, \\
 e. \quad \epsilon_{e,f} &\simeq 0.33, \\
 f.1. \quad \epsilon_{B,f,-2} &\leq 2.5 \times 10^{-4}, \\
 f.2. \quad \epsilon_{B,f,-2} &\leq 5 \times 10^{-4} & T_2^{3/4}, \\
 f.3. \quad \epsilon_{B,f,-2} &\leq 5 \times 10^{-3} & T_2^{1/2}, \\
 f.4. \quad \epsilon_{B,f,-2} &\leq 1.2 \times 10^{-2} & T_2^{5/4}, \\
 g. \quad \Gamma_{i,2.5} &\geq 0.76 & T_2^{1/8}.
 \end{aligned} \quad (12)$$

It is sufficient to meet 1 of the 4 conditions (f).

4. Numerical results

In order to obtain an accurate description of the spectrum, we have carried detailed numerical calculations of the emission of radiation from a fireball in transition to self-similar behavior. Our

²A detailed description of the derivation may be found at <http://www.weizmann.ac.il/~asaf/>

numerical model contains full description of cyclo-synchrotron emission, synchrotron self absorption, inverse- as well as direct Compton scattering, pair production and annihilation and cascade processes occurring at high energies. Full description of the model appears in Pe'er & Waxman (2003). In the present version, photons emitted after acceleration of electrons at the reverse shock, serve as seed photons for physical processes occurring after acceleration of electrons in the forward shock.

Figure 1 presents three examples of the results of our calculations, for three different sets of parameter values, consistent with the constraints derived in § 3. It demonstrates that the process described above may indeed account for the observed hard spectrum of the high energy component.

Figure 2 presents an alternative explanation to the observed high energy spectrum. The spectrum expected from internal collisions within the expanding fireball is calculated, assuming that ϵ_B and ϵ_e are similar in the two shock waves created as two plasma shells collide. The observed spectrum may be reproduced adopting rapid variability, $\Delta t_{var} \approx 10^{-5}$ s, and very low values of the equipartition fractions, $\epsilon_B \approx 10^{-7}$. Here too, the hard high energy tail is due to inverse-Compton scattering of self-absorbed synchrotron spectrum. Accounting for ~ 1 MeV GRB emission, like the variable low energy component observed at the first ~ 100 s in GRB941017, typically requires in the internal shock scenario equipartition fraction close to unity. This, and the temporal characteristics of the high energy component, suggest that the high energy tail is produced during the transition to self-similar expansion, rather than in internal shocks.

5. Discussion

We have shown that the high energy spectral component of GRB941017 may be explained as emission from shock accelerated electrons, both during the internal shock phase of fireball evolution (Figure 2) and during transition to self-similar expansion (Figure 1). In both cases, the hard spectrum is due to inverse-Compton scattering of self-absorbed synchrotron spectrum, and the magnetic field energy density in the region of inverse-Compton scattering should be well below equipartition. We consider the latter explanation, emission during transition to self-similar expansion, more viable, due to the temporal characteristics of the high energy component and due to the fact that the low energy variable component is hard to explain in the former scenario.

We have shown that the high energy data allow to put stringent constraints on fireball parameters, such as the total (isotropic equivalent) energy E , initial Lorenz factor Γ_i and ambient medium density n (Eq. 12). Such constraints can not be inferred from keV—MeV observations alone. The inferred values of E , Γ_i and n are similar to those typical to cosmological GRBs, although the inferred constraint $E/n \gtrsim 10^{56}$ erg cm³ implies a ratio E/n which is higher than typically obtained, $E/n \sim 10^{54}$ erg cm³ (Bloom, Frail & Kulkarni 2003).

The inferred values of $\epsilon_{e,f}$, $\epsilon_{B,r}$ and $\epsilon_{e,r}$ are consistent with those inferred from other GRB and afterglow observations. The value of $\epsilon_{B,f}$ is usually less well constrained by observations, and is

required to be well below equipartition in our case. This, and possibly the large ratio of E/n may account for the rareness of GRB941017-type high energy tails.

Figures 1 and 2 demonstrate that different scenarios accounting for the high energy component of GRB941017, as well as different model parameters in a given scenario, lead to different model predictions for the fluxes at optical, X-ray and sub-TeV energy bands. The fluxes predicted in Figure 1 are well within the detection capabilities of the SWIFT (in optical) and GLAST (at 10–100GeV) satellites, and of sub-TeV ground based Cerenkov telescopes (e.g. HESS (Krawczynski *et al.* 1999) , MAGIC (Petry *et al.* 1999), MILAGRO (McEnery 2003), VERITAS (Weekes *et al.* 2002)). Therefore, optical and sub-TeV observations on minute time scale will allow to put more stringent constraints on explosion parameters than those given in Eq. 12.

We thank J. Granot & D. Guetta for helpful discussions. This work was supported in part by a Minerva grant and by a grant from the Rosa and Emilio Segré fund. EW is the incumbent of the Beracha foundation career development chair.

REFERENCES

Blandford, R.D., & McKee, C.F. 1976, Phys. Fluids 19, 1130

Bloom, J. S., Frail, D. A. & Kulkarni, S. R. 2003, ApJ594, 674

Böttcher, M. & Dermer, C.D. 1998, ApJ, 499, L131

Gonzalez, M. M., *et al.* Nature, 424, 14

Granot, J. & Guetta, D. (astro-ph/0309231)

Krawczynski, H. *et al.* 1999, Bulletin of the American Astronomical Society, 31, 727

McEnery, J.E. 2003, in Gamma-ray bursts and afterglow astronomy 2001, AIP conference proceedings, 662, 529

Mészáros, P. ARA&A, 40, 137

Mészáros, P., & Rees, M.J. 1997, ApJ, 476, 232

Mészáros, P., Rees, M.J., & Papathanassiou, H. 1994, ApJ, 432, 181

Pe'er, A., & Waxman, E. 2003, in preparation

Petry, D. *et al.* 1999, A&ASuppl. Ser. 138, 601

Piran, T. 2000 Phys. Rep., 333, 529

Sari, R., & Piran, T. 1999, ApJ, 520, 641

Totani, T. 1998, ApJ 502, L13.

Waxman, E., 1995, Phys. Rev. Lett., 75, 386

Waxman, E. 1997, ApJ, 491, L19

Waxman, E. 2003, in Gamma-Ray Bursts: The Underlying Model, in Supernovae and Gamma-Ray bursters, Ed. K. Weiler (Springer), 598, 393

Waxman, E. & Bahcall, J. 2000, ApJ 541, 707.

Weekes, T.C., *et al.* 2002, Astroparticle Phys. 17, 221

Vietri, M. 1995, ApJ, 453, 883

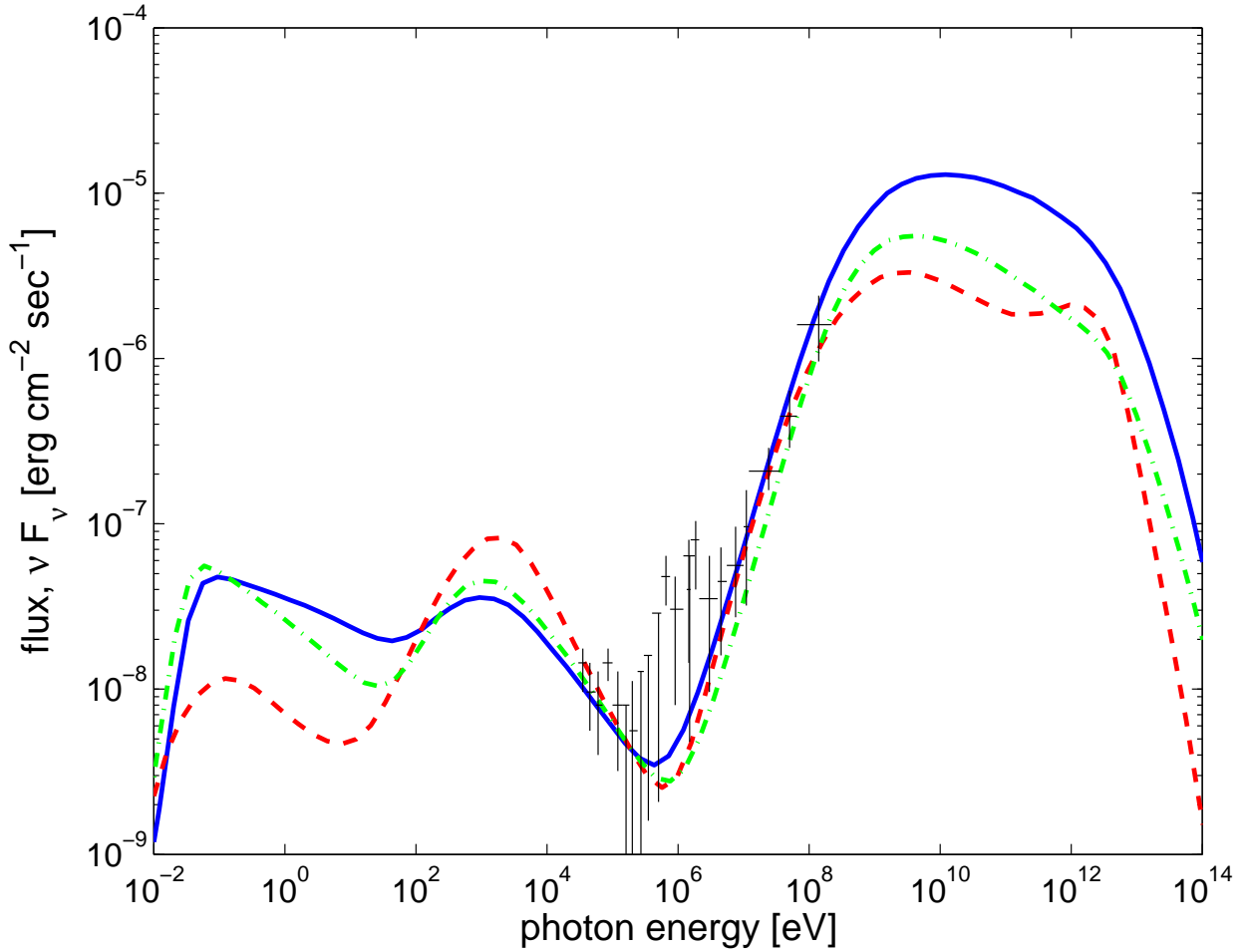


Fig. 1.— Points with error bars are the observed spectrum of GRB941017, averaged over a time interval of 100 s to 200 s following the burst trigger (González *et al.* 2003). Detailed calculations are presented for three different sets of model parameters, which are consistent with the constraints of Eq. 12: $\{E = 3 \times 10^{54} \text{ erg}, n = 0.1 \text{ cm}^{-3}, \Gamma_i = 300, \epsilon_{B,r} = 10^{-1}, \epsilon_{B,f} = 10^{-6}\}$ (solid, assumed redshift $z = 0.1$), $\{E = 10^{55} \text{ erg}, n = 0.1 \text{ cm}^{-3}, \Gamma_i = 200, \epsilon_{B,r} = 10^{-3}, \epsilon_{B,f} = 10^{-5}\}$ (dashed, assumed redshift $z = 0.25$) and $\{E = 10^{54} \text{ erg}, n = 0.03 \text{ cm}^{-3}, \Gamma_i = 220, \epsilon_{B,r} = 0.2, \epsilon_{B,f} = 3 \times 10^{-6}\}$ (dash-dotted, assumed redshift $z = 0.06$).

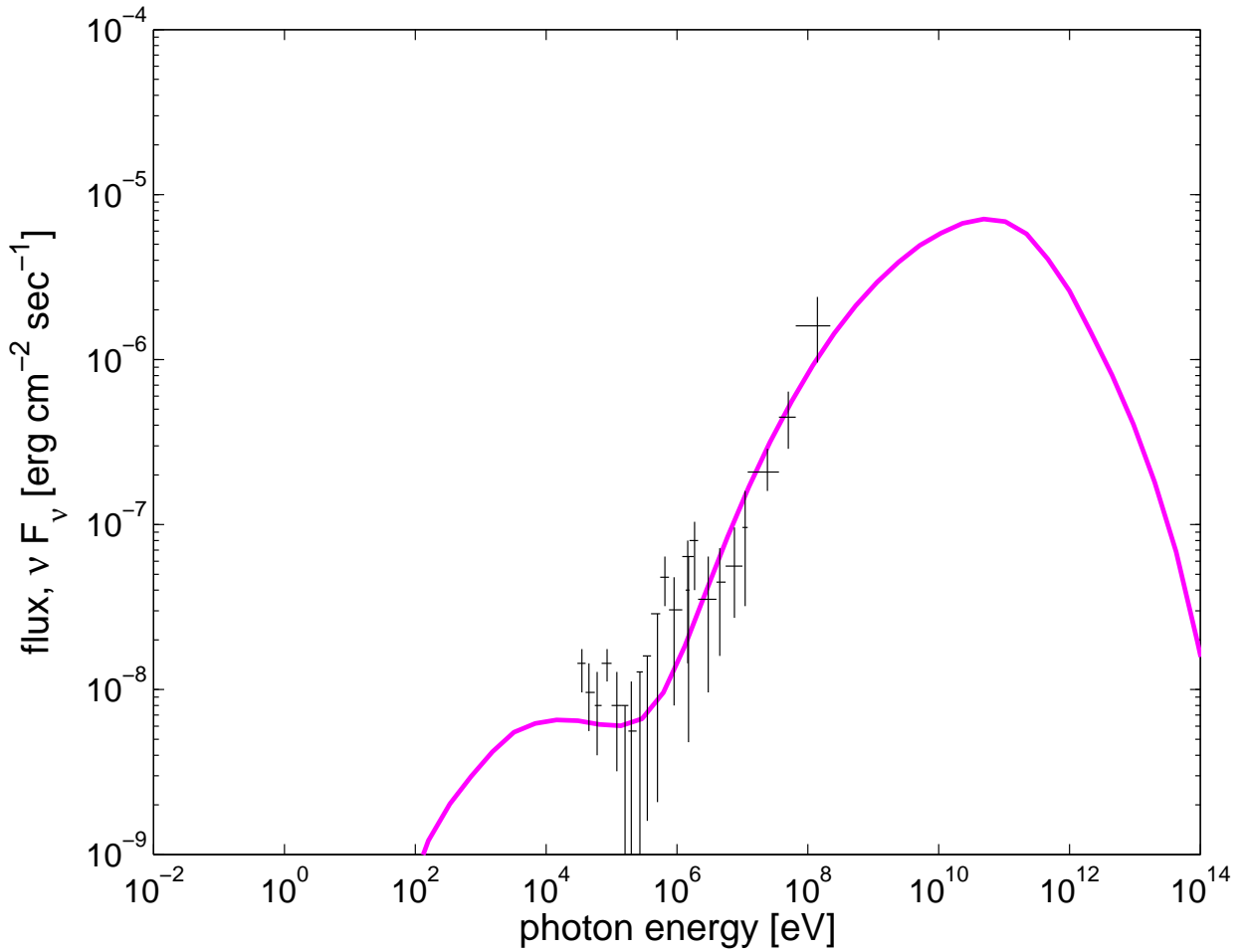


Fig. 2.— Alternative explanation of the observed high energy tail: rapid variability in prompt emission. Points with error bars are the observed spectrum of GRB941017, averaged over a time interval of 100 s to 200 s. Model parameters: $L = 3 \times 10^{52} \text{ erg s}^{-1}$, $\Delta t_{var} = 10^{-5} \text{ s}$, $\Gamma_i = 1500$, $\epsilon_{B,r} = \epsilon_{B,f} = 10^{-7}$ (assumed redshift $z=0.2$)